

# Complex coacervation: A field theoretic simulation study of polyelectrolyte complexation

Jonghoon Lee,<sup>\*</sup> Yuri O. Popov,<sup>†</sup> and Glenn H. Fredrickson<sup>‡</sup>

*Materials Research Laboratory, University of California,  
Santa Barbara, California 93106-5121*

(Dated: October 23, 2018)

## Abstract

Using the complex Langevin sampling strategy, field theoretic simulations are performed to study the equilibrium phase behavior and structure of symmetric polycation-polyanion mixtures without salt in good solvents. Static structure factors for the segment density and charge density are calculated and used to study the role of fluctuations in the electrostatic and chemical potential fields beyond the random phase approximation. We specifically focus on the role of charge density and molecular weight on the structure and complexation behavior of polycation-polyanion solutions. A demixing phase transition to form a “complex coacervate” is observed in strongly charged systems, and the corresponding spinodal and binodal boundaries of the phase diagram are investigated.

---

<sup>\*</sup>Electronic address: [jonglee@mpip-mainz.mpg.de](mailto:jonglee@mpip-mainz.mpg.de); Present address:Max Planck Institute for Polymer research, Ackermannweg 10, D-55128 Mainz, Germany

<sup>†</sup>Present address:Department of Physics, Case Western Reserve University, Cleveland, Ohio 44106

<sup>‡</sup>Department of Chemical Engineering and Materials, University of California, Santa Barbara, California 93106

## I. INTRODUCTION

Since statistical field theory was first applied to self avoiding polymers by Edwards [1], polymer field theory models and techniques have been developed and refined for a wide variety of polymeric systems [2, 3, 4, 5, 6, 7]. In the field theoretic approach, one often has to invoke approximations in order to make functional integrals for partition functions and average properties tractable. A convenient starting point is the mean field approximation, also known as *self-consistent field theory* (SCFT) [1, 4]. Since the effective coordination number grows as the square root of the molecular weight in concentrated polymeric systems, SCFT is argued to be asymptotically exact in polymeric melts when the degree of polymerization becomes infinite. Moreover, the theory serves as the reference for more sophisticated approximation schemes that attempt to account for field fluctuation effects [2, 8]. Over the last decade, with the ever increasing power of digital computation, numerical SCFT has become a routine tool for investigations of the structural and thermodynamic properties of inhomogeneous polymers, including polymer alloys and block copolymers of varying architecture [9, 10, 11].

Despite the success and the popularity of SCFT among polymer researchers, there are classes of systems where SCFT is known to be inaccurate [8]. These systems, characterized by strong or non-negligible density fluctuations, include polymer solutions in dilute and semi-dilute regimes, systems close to a phase transition, and polyelectrolyte solutions, among others. The mean field approximation (i.e. SCFT) is particularly ill-suited to polyelectrolytes; indeed, for some charged polymer systems the Coulomb interaction does not contribute to the free energy at the SCFT level. Such a system is a homogeneous polyelectrolyte solution of arbitrary concentration in the bulk. The overall charge neutrality condition of the system leads to a constant self-consistent electrostatic potential field that makes no contribution to the free energy of the solution. Hence, in such a system the electrostatics contributes to the free energy only via positional *correlations* among charges. Such charge correlations can be very strong in polyelectrolytes due to the high valency and the low translational entropy of macroions.

This strong charge correlation effect in polyelectrolytes was noticed nearly a century ago [12]: mixtures of oppositely charged biopolymers or synthetic polyelectrolytes can yield dense liquid precipitates coexisting with supernatant solvent under standard physiological

conditions at room temperature. This liquid-liquid phase separation, referred to as *complex coacervation*, is a manifestation of charge correlations and fundamentally differs from the macrophase separation that typically occurs in solutions or melts of incompatible neutral polymers. Applications of complex coacervates exist in both nature and technology. As an elegant example of the former, the “sand castle” worm constructs habitats on the meter length scale by gluing millimeter-sized grains of sand together under the sea using a wonder glue composed of anionic and cationic proteins [13]. Technological applications span the fields of water purification, adhesives, coatings, and biotechnology. For example, DNA sensors are being developed based on the complexation of target DNA molecules (anionic) with synthetic conjugated cationic polyelectrolytes [14]. Other potential applications in biotechnology relate to drug delivery and gene therapy, and invoke charge complexation to build useful structures with a payload (such as DNA) for delivery in an aqueous environment. An example of such a structure is the self-assembled polymeric micelles produced by mixing solutions of polyanions and polycations, where one or both polyelectrolytes contains a charge neutral hydrophilic block [15, 16, 17, 18]. The core of each micelle is a coacervate composed of negatively and positively charged polymer segments, while the corona consists of water soluble neutral blocks that can serve to protect the payload in the core.

Theoretically, the thermodynamics of complex coacervation was first examined by Overbeek and Voorn [19, 20]. Although they correctly identified the driving force for the phase separation as a Coulomb attraction between oppositely charged macroions, they neglected the charge connectivity along the polymer backbone and relied on the simple Debye-Hückel approximation in calculating the electrostatic free energy, which is valid only in very dilute systems [20]. Since that time, the main issue in the theory of complex coacervation has been how to properly calculate the electrostatic charge correlation in polyelectrolyte solutions. Following the maturation of polymer field theory, significant progress in our understanding of charge correlation phenomena have resulted from application of the random phase approximation (RPA) to weakly charged polyelectrolytes [21, 22, 23, 24], and loop expansions to treat stronger correlations beyond the level of the RPA [25, 26, 27]. Unfortunately these analytical techniques are still limited in scope and are particularly difficult to apply to *inhomogeneous* structures, such as mesophases.

The pervasiveness and the importance of polyelectrolyte systems in nature and biological applications, coupled with the obvious inadequacy of SCFT in describing those systems,

motivates the development of a systematic *numerical* way of incorporating field fluctuation effects beyond SCFT. Ideally, such a scheme should be capable of treating an arbitrary field theory model in the absence of any approximations (aside from numerical errors that arise from resolving and statistically sampling the fields), and thus be capable of describing strong charge and density correlation effects. Beyond serving as a general purpose simulation tool, such a “field theoretic simulation” method could be used as a test bed to validate analytical results based on loop expansions and other approximations.

Our group has developed a broad suite of methods for conducting numerical simulations of polymer statistical field theory models [28]. Since the models typically have effective Hamiltonians that are complex, rather than real, phase oscillations thwart conventional numerical simulations based on Monte Carlo sampling. We have found that this “sign problem” can be effectively treated by adopting the complex Langevin (CL) sampling method from nuclear physics [29, 30], and applying it in tandem with advanced numerical methods. This emerging field of *field theoretic simulations (FTS)* of polymeric systems has already been applied to several polymer models where SCFT is known to be inaccurate, such as block copolymers near their order-disorder transition (ODT) [31, 32], ternary blends close to a Lifshitz point [33], and polymer solutions in the semidilute regime [34, 35]. The FTS technique, however, is generic enough to be applicable to a much broader class of field theory models of complex fluids, and is potentially expandable to systems out of equilibrium [28, 36].

In this article, we report on the application of FTS to polyelectrolyte systems. Based on a field theoretic model of a simple binary polyelectrolyte mixture, FTS is used to study density correlations in the system and to directly monitor the complexation phenomena that leads to the formation of a coacervate. We recently contributed a short highlight article that included some preliminary findings [37]. Here we provide a more complete set of results, a detailed discussion of our model and numerical methods, and an in-depth analysis. A particular focus of the present paper is on charge and density correlations in the solution. Structure factors of segment density and charge density are calculated using FTS and compared with RPA structure factors.

## II. THEORY AND NUMERICAL METHODS

In this section, the field theory of our model polyelectrolyte solution is introduced. The thermodynamics of the system in the mean field approximation is studied, followed by a discussion of the first non-vanishing (RPA) correction to SCFT assuming small amplitude field fluctuations. Next, the FTS technique is described along with CL sampling. The section ends with a discussion of the numerical methods used to integrate the CL equations.

### A. Field theory model

Here we propose a simple, yet fundamental, model that is capable of giving rise to the phenomenon of complex coacervation with a minimal set of parameters. Specifically, we consider a solution consisting of a mixture of polycations and polyanions in an implicit good solvent with a uniform dielectric constant  $\epsilon$ . For simplicity, we choose to work with a *symmetric* model in which the two types of polyelectrolytes are identical except for the sign of the charge that they carry. Half of chain molecules in the system are positively charged and the other half are negatively charged, thereby preserving the condition of electroneutrality. Again, for simplicity, we do not include either counterions or salt, although such generalizations are straightforward. Our highly idealized model system, however, could be approximately realized by mixing a polyacid with a polybase of equal molecular weight and equal but opposite charge in water. We formulate our model in the canonical ensemble and consider a mixture of  $n$  polyanions and  $n$  polycations in a volume  $V$  of a three-dimensional physical space. The polymer backbones are modeled as *discrete* Gaussian (bead-spring) chains with degree of polymerization  $N$ ; the number of beads per chain is  $N + 1$ . In addition, we also employ the *continuous* Gaussian chain model to derive some analytical results in section IIC; this model is a large- $N$  limit of the discrete Gaussian chain. The charge per bead is  $+z$  for the cation species and  $-z$  for the anion species; all other physical characteristics of the two types of chains are assumed to be identical. Interactions among beads include intramolecular spring forces, and intra- and inter-molecular excluded volume and Coulomb interactions.

The classical canonical partition function of the model just described can be expressed

(in “particle” form) as

$$\mathcal{Z}_C(2n, V, T) = \frac{1}{(n!)^2 (\lambda_T^3)^{2n(N+1)}} \left( \prod_{\alpha=1}^{2n} \int d\mathbf{R}_\alpha \right) \exp[-\beta U_0 - \beta \bar{U}_{ev} - \beta \bar{U}_{es}], \quad (1)$$

where  $\lambda_T$  is the thermal de Broglie wave length for unconnected beads and  $\beta = 1/(k_B T)$  is the reciprocal of the thermal energy. In indexing chains with  $\alpha$ , the first  $n$  chains are the polyanions ( $1 \leq \alpha \leq n$ ) and the remaining  $n$  chains are the polycations ( $n+1 \leq \alpha \leq 2n$ ). The chain conformation vector  $\mathbf{R}_\alpha$  is a set of coordinates of beads belonging to chain  $\alpha$ :  $\mathbf{R}_\alpha = \{\mathbf{r}_{\alpha,0}, \mathbf{r}_{\alpha,1}, \mathbf{r}_{\alpha,2}, \dots, \mathbf{r}_{\alpha,N}\}$ . The set of bead coordinates for all  $2n$  chains is denoted by  $\mathbf{R}$ .  $\beta U_0$  is the intramolecular, short-ranged potential that connects beads along the chain backbone:

$$\beta U_0[\mathbf{R}] = \beta \sum_{\alpha=1}^{2n} \sum_{j=1}^N h(|\mathbf{r}_{\alpha,j} - \mathbf{r}_{\alpha,j-1}|). \quad (2)$$

Gaussian discrete chains are assumed with harmonic spring potential  $\beta h(r) = 3r^2/2b^2$ , where  $b$  is the length of each statistical segment.

The remaining contributions to the potential energy are potentials of mean force (denoted by an over bar) because the solvent is treated implicitly.  $\beta \bar{U}_{ev}$  is the excluded volume interaction of the system:

$$\beta \bar{U}_{ev}[\mathbf{R}] = \frac{\beta}{2} \iint d^3\mathbf{r} d^3\mathbf{r}' \hat{\rho}_n(\mathbf{r}) \bar{u}(|\mathbf{r} - \mathbf{r}'|) \hat{\rho}_n(\mathbf{r}'). \quad (3)$$

Here the microscopic segment (bead) number density operator  $\hat{\rho}_n(\mathbf{r})$  is defined as the sum of the microscopic polyanion segment density  $\hat{\rho}_-(\mathbf{r})$  and the microscopic polycation segment density  $\hat{\rho}_+(\mathbf{r})$ , where

$$\hat{\rho}_-(\mathbf{r}) = \sum_{\alpha=1}^n \sum_{j=0}^N \delta(\mathbf{r} - \mathbf{r}_{\alpha,j}) \quad (4)$$

and

$$\hat{\rho}_+(\mathbf{r}) = \sum_{\alpha=n+1}^{2n} \sum_{j=0}^N \delta(\mathbf{r} - \mathbf{r}_{\alpha,j}). \quad (5)$$

We also adopt Edwards’ simple delta function model for the volume interaction [1]:

$$\beta \bar{u}(|\mathbf{r}|) = u_0 \delta(\mathbf{r}), \quad (6)$$

where  $u_0$  is the excluded volume parameter.

The final contribution to the energy,  $\beta\bar{U}_{es}$ , is the electrostatic interaction between charges in the system:

$$\beta\bar{U}_{es}[\mathbf{R}] = \frac{1}{2} \iint d^3\mathbf{r}d^3\mathbf{r}' \hat{\rho}_c(\mathbf{r}) \frac{l_B}{|\mathbf{r} - \mathbf{r}'|} \hat{\rho}_c(\mathbf{r}'), \quad (7)$$

where  $l_B \equiv \beta e^2/\epsilon$  is a constant Bjerrum length;  $e$  is the charge of a proton. Since every bead carries charge  $+z$  or  $-z$ , the microscopic charge density is defined as

$$\hat{\rho}_c(\mathbf{r}) = -z\hat{\rho}_-(\mathbf{r}) + z\hat{\rho}_+(\mathbf{r}). \quad (8)$$

By electroneutrality, the volume integral of this microscopic charge density vanishes.

Our next step is to utilize Hubbard-Stratonovich transformation to convert the ‘‘particle’’ representation of the partition function in Eq. (1) to a more convenient statistical field theory. In this process, two auxiliary fields,  $\phi$  and  $w$ , are introduced and the partition function can be recast in the form [28]

$$\mathcal{Z}_C = \mathcal{Z}_0 \int \mathcal{D}w \int \mathcal{D}\phi \exp(-H[w, \phi]). \quad (9)$$

where the functional integrals over the two fields are taken in the real function space and  $H[w, \phi]$  is a complex effective Hamiltonian. The field  $w(\mathbf{r})$  can be interpreted as a fluctuating chemical potential field conjugate to  $\hat{\rho}_n(\mathbf{r})$ , while  $\phi(\mathbf{r})$  is an electrostatic potential field conjugate to  $\hat{\rho}_c(\mathbf{r})$ .  $\mathcal{Z}_0$  is a prefactor that includes the ideal gas entropy of non-interacting chains and some spurious self-interactions contained in Eqs. (3) and (7). These self-interactions produce only a constant shift in chemical potential and have no thermodynamic consequence. The effective Hamiltonian corresponds to the functional

$$H[w, \phi] = \frac{1}{2} \int d^3\mathbf{r} \left( \frac{[w(\mathbf{r})]^2}{u_0} + \frac{|\nabla\phi(\mathbf{r})|^2}{4\pi l_B} \right) - n \ln Q[iw + iz\phi] - n \ln Q[iw - iz\phi], \quad (10)$$

where  $Q[iw \pm iz\phi]$  is a single chain partition functional of *decoupled polyelectrolytes* in the conjugate fields. Specifically,  $Q$  is defined as the ratio of the partition function of a single chain subject to the (pure imaginary) fields  $iw(\mathbf{r}) \pm iz\phi(\mathbf{r})$  to the partition function of an ideal chain,

$$Q[iw \pm iz\phi] = \frac{\int d^3\mathbf{r}^{N+1} \exp[-\beta U_s(\mathbf{r}^{N+1})]}{V \left( \int d^3\mathbf{b} \exp[-\beta h(|\mathbf{b}|)] \right)^N}, \quad (11)$$

where  $\mathbf{r}^{N+1}$  denotes the bead coordinates of the chain and

$$\beta U_s(\mathbf{r}^{N+1}) = \sum_{j=1}^N \beta h(|\mathbf{r}_j - \mathbf{r}_{j-1}|) + i \sum_{j=0}^N [w(\mathbf{r}_j) \pm z\phi(\mathbf{r}_j)]. \quad (12)$$

The functional  $Q[iw \pm iz\phi]$  is thus normalized so that  $Q[0] = 1$ . In practice,  $Q$  is computed for an arbitrary field  $\psi(\mathbf{r})$  according to  $Q[\psi] = \frac{1}{V} \int d\mathbf{r}^3 q(\mathbf{r}, N; [\psi])$ , where  $q(\mathbf{r}, j; [\psi])$  represents the statistical weight for the  $j$ th bead of a chain to be at position  $\mathbf{r}$ . This object  $q(\mathbf{r}, j; [\psi])$ , referred to as a chain propagator, is calculated by iterating the following Chapman-Kolmogorov type equation

$$q(\mathbf{r}, j+1; [\psi]) = \left( \frac{3}{2\pi b^2} \right)^{3/2} \exp[-\psi(\mathbf{r})] \int d^3\mathbf{r}' q(\mathbf{r}', j; [\psi]) \exp\left(-\frac{3|\mathbf{r} - \mathbf{r}'|^2}{2b^2}\right) \quad (13)$$

from the initial condition of  $q(\mathbf{r}, 0; [\psi]) = \exp[-\psi(\mathbf{r})]$ . It is notable that the integral on the right hand side of Eq. (13) is of convolution form so can be efficiently evaluated using Fourier transforms.

The average of any thermodynamic observable  $\mathcal{G}$  can be formally defined as an ensemble average of the corresponding operator  $\tilde{\mathcal{G}}[w, \phi]$  over the auxiliary field variables

$$\langle \mathcal{G} \rangle = \frac{\mathcal{Z}_0}{\mathcal{Z}_C} \iint \mathcal{D}w \mathcal{D}\phi \tilde{\mathcal{G}}[w, \phi] \exp(-H[w, \phi]). \quad (14)$$

In the present paper, we are particularly interested in operators for densities of polymer segments and charges, and operators whose averages over the field variables yield two-point density and charge correlation functions. The latter can be obtained by augmenting Eq. (9) with a source term involving external fields conjugate to the microscopic segment and charge densities, and using  $\ln \mathcal{Z}_C$  as a generating functional for the cumulant moments of density [28]. The segment density operator for polycations (polyanions) is found to be

$$\tilde{\rho}_{\pm}(\mathbf{r}; [w, \phi]) \equiv -n \frac{\delta \ln Q[iw \pm iz\phi]}{\delta(iw(\mathbf{r}) \pm iz\phi(\mathbf{r}))}, \quad (15)$$

so that  $\langle \hat{\rho}_{\pm}(\mathbf{r}) \rangle = \langle \tilde{\rho}_{\pm}(\mathbf{r}; [w, \phi]) \rangle$ . In practice, the functional derivative on the right hand side of Eq. (15) can be computed using the chain propagator  $q$  as

$$\frac{\delta \ln Q[\psi]}{\delta \psi(\mathbf{r})} = -\frac{\exp(\psi)}{VQ[\psi]} \sum_{j=0}^N q(\mathbf{r}, N-j; [\psi]) q(\mathbf{r}, j; [\psi]). \quad (16)$$

The total segment number density operator  $\tilde{\rho}_n(\mathbf{r})$  is the sum of  $\tilde{\rho}_+(\mathbf{r})$  and  $\tilde{\rho}_-(\mathbf{r})$ :

$$\tilde{\rho}_n(\mathbf{r}; [w, \phi]) = \tilde{\rho}_+(\mathbf{r}; [w, \phi]) + \tilde{\rho}_-(\mathbf{r}; [w, \phi]). \quad (17)$$



Likewise, the charge density operator  $\tilde{\rho}_c(\mathbf{r})$  is the sum of  $\tilde{\rho}_+(\mathbf{r})$  and  $\tilde{\rho}_-(\mathbf{r})$  weighted by the respective charge densities:

$$\tilde{\rho}_c(\mathbf{r}; [w, \phi]) = z \{ \tilde{\rho}_+(\mathbf{r}; [w, \phi]) - \tilde{\rho}_-(\mathbf{r}; [w, \phi]) \}. \quad (18)$$

The correlations in the density fluctuations can be formally related to the correlation functions of the corresponding auxiliary fields. The pair correlation function of total segment number density can be computed from the pair correlation function of the auxiliary chemical potential field according to

$$\langle \hat{\rho}_n(\mathbf{r}) \hat{\rho}_n(\mathbf{r}') \rangle = \frac{\delta(\mathbf{r} - \mathbf{r}')}{u_0} - \frac{\langle w(\mathbf{r}) w(\mathbf{r}') \rangle}{u_0^2}. \quad (19)$$

The charge density correlation function can be similarly related to the pair correlation function of the auxiliary electrostatic potential field

$$\langle \hat{\rho}_c(\mathbf{r}) \hat{\rho}_c(\mathbf{r}') \rangle = \frac{-\nabla^2 \delta(\mathbf{r} - \mathbf{r}')}{4\pi l_B} - \frac{\langle \nabla^2 \phi(\mathbf{r}) \nabla^2 \phi(\mathbf{r}') \rangle}{(4\pi l_B)^2}. \quad (20)$$

The cross correlation between the segment number density and the charge density is similarly given by

$$\langle \hat{\rho}_n(\mathbf{r}) \hat{\rho}_c(\mathbf{r}') \rangle = \frac{\langle w(\mathbf{r}) \nabla^2 \phi(\mathbf{r}') \rangle}{u_0 4\pi l_B}. \quad (21)$$

The microstructure of the polyelectrolyte solution can be characterized with static structure factors, which are related to the pair correlation functions by Fourier transforms. The number density structure factor, defined as

$$S_{nn}(k) = \frac{1}{V} \iint d^3\mathbf{r} d^3\mathbf{r}' \exp[-i\mathbf{k} \cdot (\mathbf{r} - \mathbf{r}')] \langle \hat{\rho}_n(\mathbf{r}) \hat{\rho}_n(\mathbf{r}') \rangle, \quad (22)$$

can be evaluated formally from Eq. (19) in terms of the  $w$  field pair correlation function

$$S_{nn}(k) = \frac{1}{u_0} - \frac{\langle \hat{w}(\mathbf{k}) \hat{w}(-\mathbf{k}) \rangle}{u_0^2 V} \quad (23)$$

for  $k \neq 0$ , where  $\hat{w}(\mathbf{k})$  is the Fourier transform of  $w(\mathbf{r})$ . Likewise, the static structure factor for the charge density can be calculated from the  $\phi$  field pair correlation function as

$$S_{cc}(k) = \frac{k^2}{4\pi l_B} - \left( \frac{k^2}{4\pi l_B} \right)^2 \frac{\langle \hat{\phi}(\mathbf{k}) \hat{\phi}(-\mathbf{k}) \rangle}{V}, \quad (24)$$

where  $\hat{\phi}(\mathbf{k})$  is the Fourier transform of  $\phi(\mathbf{r})$ . The structure factor for the cross correlation between the segment number density and the charge density can be calculated from the correlation between the  $w(\mathbf{r})$  field fluctuation and the  $\phi(\mathbf{r})$  field fluctuation,

$$S_{nc}(k) = -\frac{k^2}{u_0 4\pi l_B} \frac{\langle \hat{w}(\mathbf{k}) \hat{\phi}(-\mathbf{k}) \rangle}{V}. \quad (25)$$

## B. Self consistent field theory

Self-consistent field theory (SCFT) is derived by assuming that the functional integrals of Eqs. (9) and (14) are dominated by “mean field” configurations  $w^*(\mathbf{r})$  and  $\phi^*(\mathbf{r})$  that correspond to saddle points of the effective Hamiltonian. The saddle point conditions produce the following SCFT equations:

$$\left. \frac{\delta H}{\delta w} \right|_{\substack{w=w^* \\ \phi=\phi^*}} = 0 \longrightarrow \frac{w^*(\mathbf{r})}{u_0} + i\tilde{\rho}_n(\mathbf{r}; [w^*, \phi^*]) = 0 \quad (26)$$

and

$$\left. \frac{\delta H}{\delta \phi} \right|_{\substack{w=w^* \\ \phi=\phi^*}} = 0 \longrightarrow \frac{-\nabla^2 \phi^*(\mathbf{r})}{4\pi l_B} + i\tilde{\rho}_c(\mathbf{r}; [w^*, \phi^*]) = 0. \quad (27)$$

The electrostatic mean field Eq. (27) recovers the conventional Poisson equation with  $i\phi^*$  interpreted as the electrostatic potential. Indeed, the physically relevant solutions of these equations correspond to  $w^*$  and  $\phi^*$  being pure imaginary fields. In an unbounded system, or a system with periodic boundary conditions imposed on both  $w(\mathbf{r})$  and  $\phi(\mathbf{r})$ , and under good solvent conditions  $u_0 > 0$ , these equations yield only *homogeneous* saddle fields of constant (imaginary)  $w^*$  and  $\phi^*$ . This trivial mean field solution corresponds to  $\nabla\phi^* = 0$  and  $w^* = -iu_0\rho_0$ , where  $\rho_0$  is the average segment number density,  $2n(N+1)/V$ .

At the SCFT level of description, our model system is thus a structureless polymer solution with constant segment density and a trivial structure factor,  $S_{nn}(k) = u_0^{-1}$ . The overall electro-neutrality makes the charge density vanish locally, because the constant positive charge density field is compensated by the constant negative charge density field. The Helmholtz free energy  $A$  thus involves only the ideal gas translational entropy and the excluded volume interaction, and is minimal when polymer chains are evenly distributed in the system:

$$\begin{aligned} \beta A &= -\ln \mathcal{Z}_C \approx -\ln \mathcal{Z}_0 + H[w^*, \phi^*] \\ &= \beta A_0 + \frac{u_0}{2} \rho_0^2 V, \end{aligned} \quad (28)$$

where  $\beta A_0 = -\ln \mathcal{Z}_0$  is the ideal chain (translational entropy) term. Therefore, there is no contribution of the Coulomb interaction to the mean field free energy, and SCFT is unable to predict the formation of a complex coacervate.

### C. Gaussian fluctuations

The phenomenon of coacervation can be traced to the presence of charge correlations in polyelectrolyte mixtures – correlations that are neglected in the mean field approximation. This correlation effect can be treated analytically with the systematic loop expansion scheme. The first correction to SCFT in such a loop expansion can be calculated analytically for our model system under the assumptions of continuous (rather than discrete) Gaussian chains and weak (low amplitude) field fluctuations. Later, the correlation functions calculated in this subsection will be compared with FTS results for discrete Gaussian chains with varying degrees of polymerization  $N$  and for arbitrary strengths of field fluctuations.

For the case of a polymer that is experiencing an arbitrary field  $\psi(\mathbf{r})$  that fluctuates only weakly from its homogeneous mean field  $\psi^*$ , the single chain partition function  $Q[\psi]$  for a continuous Gaussian chain can be approximated up to the second order in field fluctuation as [28]

$$Q[\psi] \approx \exp[-N\hat{\psi}(0)/V] \times \left\{ 1 + \frac{N^2}{2V^2} \sum_{\mathbf{k} \neq 0} \hat{g}_D(k^2 R_g^2) \hat{\psi}(\mathbf{k}) \hat{\psi}(-\mathbf{k}) + \mathcal{O}(\hat{\psi}^3) \right\}, \quad (29)$$

where  $\hat{\psi}(\mathbf{k})$  is the Fourier transform of  $\psi(\mathbf{r})$ , and  $R_g = b\sqrt{N/6}$  is the radius of gyration of a Gaussian chain without interactions. The Debye function  $\hat{g}_D(k^2 R_g^2)$  is the scattering function of an ideal continuous Gaussian chain [38]:

$$\hat{g}_D(x) = \frac{2}{x^2} [\exp(-x) + x - 1]. \quad (30)$$

With Eq. (29), the effective Hamiltonian of Eq. (10) can be approximated as

$$H[w, \phi] \approx H[w^*, \phi^*] + \frac{1}{2V} \sum_{\mathbf{k} \neq 0} \left[ \hat{\gamma}_{ww}(k) \hat{w}(\mathbf{k}) \hat{w}(-\mathbf{k}) + \hat{\gamma}_{\phi\phi}(k) \hat{\phi}(\mathbf{k}) \hat{\phi}(-\mathbf{k}) \right], \quad (31)$$

where fluctuations of  $w$  and  $\phi$  fields are decoupled at quadratic order with expansion coefficients of

$$\hat{\gamma}_{ww}(k) = \frac{1}{u_0} + \rho_0 N \hat{g}_D(k^2 R_g^2) \quad (32)$$

and

$$\hat{\gamma}_{\phi\phi}(k) = \frac{k^2}{4\pi l_B} + \rho_0 N z^2 \hat{g}_D(k^2 R_g^2). \quad (33)$$

Using Eqs. (9) and (31), the osmotic pressure  $p$  of the solution with weak Gaussian field fluctuations can be approximated as

$$\begin{aligned} \beta p &= -\left(\frac{\partial \beta A}{\partial V}\right)_{n,\beta} = \left(\frac{\partial \ln \mathcal{Z}_C}{\partial V}\right)_{n,\beta} \\ &\approx \frac{\rho_0}{N} + \frac{u_0 \rho_0^2}{2} - \frac{1}{24\pi} \left[ \left(\frac{12u_0 \rho_0}{b^2}\right)^{3/2} + \frac{1}{\sqrt{2}} \left(\frac{48\pi l_B z^2 \rho_0}{b^2}\right)^{3/4} \right], \end{aligned} \quad (34)$$

where the last negative term with square brackets is the correction to the mean field osmotic pressure due to field fluctuation effects. Eqn. (34) can be expressed in a dimensionless form,

$$\beta p R_g^3 \approx C + \frac{BC^2}{2} - \frac{1}{24\pi} \left[ (2BC)^{3/2} + \frac{(2EC)^{3/4}}{\sqrt{2}} \right], \quad (35)$$

with reduced (dimensionless) variables of

$$C = \frac{2nR_g^3}{V}, \quad B = \frac{u_0 N^2}{R_g^3}, \quad E = \frac{4\pi l_B z^2 N^2}{R_g}, \quad (36)$$

where  $C$  is a reduced chain concentration,  $B$  is a reduced excluded volume parameter, and  $E$  is a reduced Bjerrum length.

The comparison between contributions from the mean field and the correction due to field fluctuations in Eq. (35) provides a criterion that can be used to assess the importance of field fluctuations. For the excluded volume interaction, the  $w$  field fluctuation can be regarded as weak correction when

$$BC^2 \gg (BC)^{3/2}. \quad (37)$$

Therefore, in a three dimensional physical space, the mean field result becomes asymptotically exact when  $C/B \gg 1$ <sup>1</sup>. In contrast, the electrostatic  $\phi$  field fluctuation contribution, namely the term scaling like  $-(EC)^{3/4}$ , is of paramount importance because there is no contribution from the mean electrostatic field to the osmotic pressure. Thus, electrostatic

---

<sup>1</sup> While the condition  $C/B \gg 1$  is commonly identified as the definition of the dense regime for neutral polymer solutions [28, 34], we note that the precise account of the numerical prefactors in Eq. (35) produces a slightly different condition:  $C/B \gg 1/18\pi^2 \approx 1/178$ . The numerical factor  $1/18\pi^2$  lowers the formal boundary between the dense and the semi-dilute regimes by more than two orders of magnitude. For this reason we call the case of  $C = 1$  and  $B = 12$  (discussed below) as “moderately dense” rather than “semi-dilute”, as this case may be interpreted as being on either side of the formal boundary between the dense and the semi-dilute regimes depending on the exact condition applied.

correlation effects can be neglected only when  $(EC)^{3/4}$  is small compared with all other contributions to the osmotic pressure. Because the electrostatic mean-field term is identically zero, a criterion similar to Eq. (37) cannot be derived from Eq. (35), and hence the range of validity of the electrostatic term is unknown at the one-loop (Gaussian) level. Evaluation of higher order terms in a loop expansion would be required to clarify the range of validity of this term.

It is important to note that Eq. (35) predicts a *negative (attractive)* contribution of electrostatic correlations to the osmotic pressure. This contribution, which is similar to expressions derived previously using the RPA [21, 22, 23, 24, 25, 26, 27], can drive complexation of polyanions and polycations to produce a complex coacervate phase. As will be discussed below, the polymer concentration in the coacervate can be estimated by balancing the repulsive excluded volume terms and the attractive electrostatic correlation terms in Eq. (35).

Using auxiliary field pair correlations calculated with the quadratic Hamiltonian of Eq. (31), structure factors of the segment density  $S_{nn}(k)$  and charge density  $S_{cc}(k)$  can be approximated by expressions involving the quadratic expansion coefficients of Eq. (32) and Eq. (33) [28]:

$$S_{nn}(k) \approx \frac{1}{u_0} - \frac{1}{u_0^2 \hat{\gamma}_{ww}(k)} \quad (38)$$

and

$$S_{cc}(k) \approx \frac{k^2}{4\pi l_B} - \left( \frac{k^2}{4\pi l_B} \right)^2 \frac{1}{\hat{\gamma}_{\phi\phi}(k)}. \quad (39)$$

These structure factors are commonly referred to as RPA structure factors and are applicable in the weak field fluctuation limit of Eq. (31) where the harmonic fluctuations in the  $w$  and  $\phi$  fields are decoupled. Indeed, the structure factor for the cross correlation between the number density and the charge density  $S_{nc}(k)$  vanishes in this level of description, as the approximated Hamiltonian of Eq. (31) does not involve a term proportional to  $\hat{w}(\mathbf{k})\hat{\phi}(-\mathbf{k})$ . Complex coacervation is a phase transition that occurs when the charge density correlations are strong enough to influence the segment density distribution. Therefore, it would seem that structure factors must be calculated beyond the RPA level to accurately describe the complexation process [25].

#### D. Field theoretic simulations

The analytic treatment of field fluctuation effects in the previous subsection is based on the weak inhomogeneity approximation of Eqs. (29) and (31). Here we turn to a direct numerical approach (FTS) that avoids any assumption of weak field fluctuations.

The essence of FTS is to devise an efficient numerical strategy of multi-dimensional integration whereby thermodynamic averages defined in Eq. (14) can be evaluated. The conventional Monte Carlo importance sampling strategy is problematic for that purpose. Although the functional integrals in Eq. (14) are over strictly real functions  $w(\mathbf{r})$  and  $\phi(\mathbf{r})$ , the effective Hamiltonian  $H[w, \phi]$  is a complex functional. Therefore, the probability weight proportional to  $\exp(-H[w, \phi])$  is not positive definite unless the sampling trajectory happens to be along a constant phase path of  $\exp(-H[w, \phi])$ . Because the identification of constant phase paths in high dimensional function spaces is computationally unfeasible, a fundamentally different simulation technique is required.

The complex Langevin (CL) sampling strategy addresses the so-called ‘‘sign problem’’ associated with the non-positive definite statistical weight of the field theory [29, 30]. The idea behind this method is to extend the real fields into the complex plane and to compute ensemble averages of observable quantities by sampling fields along a stationary stochastic trajectory in the complex function space. By extending the real fields  $w(\mathbf{r})$  and  $\phi(\mathbf{r})$  into the complex functions  $W(\mathbf{r}) = w(\mathbf{r}) + iw_I(\mathbf{r})$  and  $\Phi(\mathbf{r}) = \phi(\mathbf{r}) + i\phi_I(\mathbf{r})$ , the ensemble average of Eq. (14) can be reexpressed as

$$\langle \mathcal{G} \rangle = \iiint \mathcal{D}w \mathcal{D}w_I \mathcal{D}\phi \mathcal{D}\phi_I \tilde{\mathcal{G}}[W, \Phi] P[w, w_I, \phi, \phi_I], \quad (40)$$

where  $P[w, w_I, \phi, \phi_I]$  is a *real non-negative* statistical distribution of fields replacing the complex weight of Eq. (14). This comes at the cost of doubling the number of the configurational degrees of freedom [28]:

$$\frac{\mathcal{Z}_0 e^{-H[w', \phi']}}{\mathcal{Z}_C} = \iiint \mathcal{D}w \mathcal{D}w_I \mathcal{D}\phi \mathcal{D}\phi_I \delta[w' - w - iw_I] \delta[\phi' - \phi - i\phi_I] P[w, w_I, \phi, \phi_I], \quad (41)$$

where  $w'$  and  $\phi'$  are real fields. Although necessary and sufficient conditions for the existence of  $P$  satisfying Eq. (41) given a complex effective Hamiltonian  $H$  have been identified [39, 40], these conditions are difficult to verify in the highly nonlinear and nonlocal Hamiltonians of polymer field theory. However, the current and the previous successful applications of the CL method to polymer models provide such a proof *a posteriori* [34, 35, 41].

The CL dynamics is a stochastic Langevin dynamics in the complex function space designed to generate a stationary Markov sequence of complex functions with distribution  $P[w, w_I, \phi, \phi_I]$ :

$$\begin{aligned} \frac{\partial}{\partial t} W(\mathbf{r}, t) &= -\lambda_w \left[ \frac{\delta H[W, \Phi]}{\delta W(\mathbf{r}, t)} \right] + \eta_w(\mathbf{r}, t) \\ &= -\lambda_w \left[ \frac{W(\mathbf{r}, t)}{u_0} + i\tilde{\rho}_n(\mathbf{r}, t; [W, \Phi]) \right] + \eta_w(\mathbf{r}, t) \end{aligned} \quad (42)$$

and

$$\begin{aligned} \frac{\partial}{\partial t} \Phi(\mathbf{r}, t) &= -\lambda_\phi \left[ \frac{\delta H[W, \Phi]}{\delta \Phi(\mathbf{r}, t)} \right] + \eta_\phi(\mathbf{r}, t) \\ &= -\lambda_\phi \left[ \frac{-\nabla^2 \Phi(\mathbf{r}, t)}{4\pi l_B} + i\tilde{\rho}_c(\mathbf{r}, t; [W, \Phi]) \right] + \eta_\phi(\mathbf{r}, t), \end{aligned} \quad (43)$$

where  $\eta_w(\mathbf{r}, t)$  and  $\eta_\phi(\mathbf{r}, t)$  are *real* Gaussian white noise fields with zero mean and variances proportional to the real dissipative coefficients  $\lambda_w$  and  $\lambda_\phi$ , respectively, consistent with the familiar fluctuation-dissipation theorem of Brownian dynamics [28]. The CL equations should be interpreted as a *fictitious*, rather than physical, dynamics to sample the field configuration space. In the absence of the random forces, the above equations reduce to deterministic equations that have saddle point field configurations of Eq. (26) and Eq. (27) as steady state solutions. With the forcing terms, the stochastic dynamics drive trajectories in the complex function space that produce steady distributions  $P[w, w_I, \phi, \phi_I]$  that are peaked at saddle point configurations. Because the random forces are strictly real, the imaginary components of the CL dynamics drive the field trajectories towards constant phase paths, while the real components of the equations are responsible for stochastic motion along a path. Under conditions where a stationary distribution is achieved, the ensemble average of Eq. (40) can be approximated by a time average along the CL trajectory.

In the numerical application of CL dynamics to affect a field-theoretic simulation, physical space and time are both discretized. For bulk simulations with periodic boundary conditions imposed on the fields, we have found that the spatial discretization is most conveniently accomplished by spectral collocation using a plane wave basis and a uniform computational grid of  $M$  sites [42]. Fast Fourier transforms (FFTs) can then be used to efficiently switch between real space (i.e. an  $M$ -vector of field values on the grid sites) and Fourier space (i.e. the first  $M$  Fourier coefficients) representations of the fields.

Upon spectral collocation, the continuum CL Eqs. (42) and (43) are transformed into a set of  $4M$  stochastic differential equations that can be integrated forward in time from

an initial field configuration by standard algorithms [43, 44]. The simplest algorithm is the explicit Euler-Maruyama time integration scheme,

$$\mathbf{W}^{(t+\Delta t)} = \mathbf{W}^{(t)} - \lambda_w \Delta t (\Delta x)^3 \left( \frac{\mathbf{W}^{(t)}}{u_0} + i \boldsymbol{\rho}_n^{(t)} \right) + \mathbf{R}_w^{(t)} \quad (44)$$

and

$$\boldsymbol{\Phi}^{(t+\Delta t)} = \boldsymbol{\Phi}^{(t)} - \lambda_\phi \Delta t (\Delta x)^3 \left( \frac{-\nabla^2 \boldsymbol{\Phi}^{(t)}}{4\pi l_B} + i \boldsymbol{\rho}_c^{(t)} \right) + \mathbf{R}_\phi^{(t)}, \quad (45)$$

where  $\Delta x$  is the grid spacing used for the spacial discretization, and  $\Delta t$  is the time spacing used for the temporal discretization. Here,  $\mathbf{W}$ ,  $\boldsymbol{\Phi}$ ,  $\boldsymbol{\rho}_n$ , and  $\boldsymbol{\rho}_c$  are  $M$ -vectors of complex variables, which represent the collocated values of the fields  $W(\mathbf{r})$ ,  $\Phi(\mathbf{r})$ ,  $\tilde{\rho}_n(\mathbf{r})$ , and  $\tilde{\rho}_c(\mathbf{r})$  on the computational grid. The superscripts index the discrete time at which the  $M$ -vectors are evaluated.  $\mathbf{R}_w^{(t)}$  and  $\mathbf{R}_\phi^{(t)}$  are  $M$ -vectors of real Gaussian random variables, which are obtained by spatial collocation of the continuous functions  $R_w(\mathbf{r}, t)$  and  $R_\phi(\mathbf{r}, t)$  defined by

$$R_w(\mathbf{r}, t) \equiv \int_t^{t+\Delta t} d\tau \eta_w(\mathbf{r}, \tau) \quad (46)$$

and

$$R_\phi(\mathbf{r}, t) \equiv \int_t^{t+\Delta t} d\tau \eta_\phi(\mathbf{r}, \tau). \quad (47)$$

The grid-collocated fields  $\mathbf{R}_w$  and  $\mathbf{R}_\phi$  are Gaussian white noise functions with vanishing averages,  $\langle \mathbf{R}_w^{(t)} \rangle = \langle \mathbf{R}_\phi^{(t)} \rangle = 0$ , second moments given by

$$\langle \mathbf{R}_w^{(t)} \mathbf{R}_w^{(t')} \rangle = 2\lambda_w \Delta t \delta_{t,t'} \mathbf{1} \quad (48)$$

$$\langle \mathbf{R}_\phi^{(t)} \mathbf{R}_\phi^{(t')} \rangle = 2\lambda_\phi \Delta t \delta_{t,t'} \mathbf{1} \quad (49)$$

and vanishing cross-correlations. The rank  $M$  unit tensor is denoted by  $\mathbf{1}$ .

Stochastic time integration algorithms for the CL equations lead to time discretization errors in computed expectation values that scale as a power of the time step  $\Delta t$ . The Euler-Maruyama (EM) scheme summarized by Eqs. (44) and (45) is of weak order one, which implies that the errors in computed averages vanish as  $\Delta t$  for small  $\Delta t$ . This low order accuracy and the poor stability characteristics of the Euler-Maruyama algorithm make it unsuitable for the large-scale 3d simulations reported here. We have instead adopted a semi-implicit, weak second order algorithm developed by Lennon and coworkers [45], which was itself inspired by operator splitting methods devised by Petersen and Öttinger [44, 46]. Beyond the second order accuracy, the Lennon algorithm utilizes analytic information about



the linearized force in a semi-implicit update scheme to improve stability. The algorithm can be cast in a predictor-corrector form with the field updates conducted in Fourier space (discrete Fourier transforms of the collocated fields are denoted by carets). The predictor steps are explicit EM updates of Eq. (44) and Eq. (45) in Fourier space:

$$\hat{\mathbf{W}}^{(*)} = \hat{\mathbf{W}}^{(t)} - \Delta_w \left( \frac{\hat{\mathbf{W}}^{(t)}}{u_0} + i\hat{\rho}_n^{(t)} \right) + \hat{\mathbf{R}}_w^{(t)} \quad (50)$$

and

$$\hat{\Phi}^{(*)} = \hat{\Phi}^{(t)} - \Delta_\phi \left( \frac{k^2 \hat{\Phi}^{(t)}}{4\pi l_B} + i\hat{\rho}_c^{(t)} \right) + \hat{\mathbf{R}}_\phi^{(t)}, \quad (51)$$

where the parameters  $\Delta_w$  and  $\Delta_\phi$  are defined as  $\Delta_w \equiv \lambda_w \Delta t (\Delta x)^3$  and  $\Delta_\phi \equiv \lambda_\phi \Delta t (\Delta x)^3$ .

The corrector steps are

$$\hat{\mathbf{W}}^{(t+\Delta t)} = \frac{\hat{\mathbf{W}}^{(t)} + [1 + \Delta_w \rho_0 N \hat{g}_D(k^2 R_g^2)] \hat{\mathbf{W}}^{(*)} - \Delta_w i\hat{\rho}_n^{(*)} + \hat{\mathbf{R}}_w^{(t)}}{2 + \Delta_w \hat{\gamma}_{ww}(k)} \quad (52)$$

and

$$\hat{\Phi}^{(t+\Delta t)} = \frac{\hat{\Phi}^{(t)} + [1 + \Delta_\phi \rho_0 N z^2 \hat{g}_D(k^2 R_g^2)] \hat{\Phi}^{(*)} - \Delta_\phi i\hat{\rho}_c^{(*)} + \hat{\mathbf{R}}_\phi^{(t)}}{2 + \Delta_\phi \hat{\gamma}_{\phi\phi}(k)}, \quad (53)$$

where  $\hat{\rho}_n^{(*)}$  and  $\hat{\rho}_c^{(*)}$  are the segment number density and the charge density operators based on the predicted fields of  $\hat{\Phi}^{(*)}$  and  $\hat{\mathbf{W}}^{(*)}$ .

This improved stochastic integration algorithm was recently applied to FTS-CL simulations of block copolymer melts and has been extensively tested in that context by Lennon and coworkers [45]. In the present case of polyelectrolyte solutions, we have found that the Lennon algorithm permits the use of a time step that is an order of magnitude larger than that mandated by stability for the EM algorithm. This translates to a ten-fold reduction in computational time.

In the following section, the FTS results are discussed in the context of the dimensionless parameters introduced in Eq. (36):  $B$ ,  $C$  and  $E$ . These parameters appear naturally in the field theory if all lengths are scaled by the radius of gyration  $R_g$ , the  $W$  field is rescaled according to  $\tilde{W} = NW$ , and the  $\Phi$  field is rescaled as  $\tilde{\Phi} = zN\Phi$ . With these scalings, the CL equations (50)-(53) for *continuous* polymer chains depend on the three intensive model parameters ( $B$ ,  $C$ ,  $E$ ), the dimensionless simulation cell size  $\tilde{L} = L/R_g$ , and on three dimensionless parameters that relate to the spatial and temporal resolution of the numerical algorithm:

$$\tilde{\Delta x} = \Delta x / R_g \quad (54)$$

$$(\Delta t)_w = \lambda_w N^2 \Delta t \quad (55)$$

$$(\Delta t)_\phi = \lambda_\phi N^2 z^2 \Delta t \quad (56)$$

For *discrete* polymer chains, the number of segments  $N$  appears as an additional independent parameter in the update equations. However, we shall see that its influence is diminished as  $N$  is increased to large values approaching the continuous polymer limit.

At fixed spatial resolution with the Lennon algorithm, we expect second-order convergence in average properties as the parameters  $(\Delta t)_w$  and  $(\Delta t)_\phi$  are reduced. All simulation data reported below were obtained by setting  $(\Delta t)_w$  and  $(\Delta t)_\phi$  to values such that the time integration error was negligible compared to the statistical sampling error. In contrast, due to ultraviolet divergences in the continuum field theory [28, 35], we do not expect convergence of certain average properties (such as absolute chemical potentials) as the spatial grid spacing  $\widetilde{\Delta x}$  is refined. However, the structure factors and phase boundaries studied here were found to be devoid of ultraviolet divergences, so no special regularization procedures were required to isolate the singularities.

### III. RESULTS AND DISCUSSION

In this section, we summarize and discuss FTS results for the field theory model formulated in the previous section in the parameter space of  $B$ ,  $C$ , and  $E$ . While these three parameters completely determine the intensive thermodynamic properties of a system comprised of continuous Gaussian chains, as discussed above, there is an additional independent parameter for the discrete Gaussian chains employed in the simulations – the degree of polymerization  $N$ . We begin with homogeneous solutions of *neutral* polymers corresponding to  $E = 0$ . The effect of the strength of the excluded volume interaction ( $B$ ) and the degree of polymerization ( $N$ ) on segment density correlations are studied using FTS, and compared with the RPA structure factor. While studying the effect of  $N$ , the parameters  $C$  and  $B$  are maintained at constant values. Next, we discuss the effect of the parameter  $E$  on density correlations and charge correlations in oppositely charged polyelectrolyte solutions with fixed  $B$ ,  $C$ , and  $N$ . Finally, we construct the phase diagram of our model system in a restricted region of the parameter space. Although a more comprehensive study of the phase

diagram is worthy to pursue, the high dimensionality of the parameter space and the significant computational requirements both limit the scope of our investigation. Nonetheless, our results shall serve to highlight the power and capability of FTS in addressing difficult problems in polyelectrolyte complexation.

The cubic simulation box applied in our simulations has a volume  $V$  of  $(4R_g)^3$  ( $\tilde{L} = 4$ ) and is subject to periodic boundary conditions. Occasionally, a larger simulation box with  $V$  of  $(8R_g)^3$  was used to confirm that finite size effects were not influencing structure or thermodynamics. In discretizing the simulation volume,  $\Delta x$  is desired to be smaller than the physical length scales of interest (i.e. the correlation lengths for the two fields), but an excessively small  $\Delta x$  adds significantly to the computational cost. In most of our simulations,  $\Delta x$  was chosen to be  $R_g/8$ , so the volume of  $(4R_g)^3$  corresponds to a lattice with  $M = 32^3$  sites. Unlike  $\Delta x$ , which was fixed,  $\Delta t$  was varied over a broad range to achieve a consistent accuracy of time integration depending on the strength of field fluctuations around the mean field:  $(\Delta t)_{w,\phi} \in [0.001, 0.1]$ . The correlation time is also highly variable throughout parameter space. Typically,  $10^4$  statistically independent field configurations were sampled to calculate averages, which corresponds to a number of time steps in the range of  $5 \times 10^4$  to  $5 \times 10^5$ . The calculation of each structure-factor curve reported here takes from 4 days to 7 weeks of CPU time on a single AMD Opteron 248 processor (2.2GHz). However, the algorithm scales nearly linearly with domain decomposition across multiple processors, so the simulations reported here are ideally suited for a parallel computing environment.

### A. The segment density correlation in neutral polymer solutions

By setting the charge on the polymer segments to zero ( $z = E = 0$ ), our model system becomes a solution of electrically neutral polymers in a good solvent. This is the Edwards' model [1] (Model A of Ref. [28]). When the  $w$  field fluctuations are weak, by application of Eqs. (32) and (36), the segment structure factor of Eq. (38) can be approximated by the dimensionless form,

$$u_0 S_{nn}(k) \approx \frac{BC \hat{g}_D(k^2 R_g^2)}{1 + BC \hat{g}_D(k^2 R_g^2)}, \quad (57)$$

which indicates that the structure factor of segment density is completely determined by one parameter, the product of  $B$  and  $C$ . In deriving this analytical formula, the chain

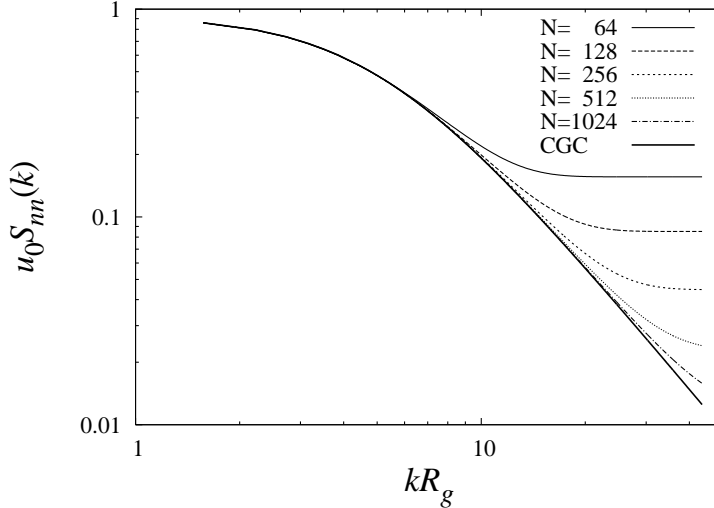


FIG. 1: RPA structure factor for the segment density when  $BC = 12$ . Segment structure factors for several values of  $N$ , calculated from Eq. (58), are compared with the result based on the continuous Gaussian chain (CGC), cf. Eq. (57).

molecules were assumed to be continuous Gaussian chains (CGCs), thus the Debye function  $\hat{g}_D(k^2 R_g^2)$  depends only on the unperturbed radius of gyration  $R_g$ . However, our simulations were conducted using *discrete* Gaussian chains (DGCs) with  $N$  segments on each chain, for which the corresponding Debye functions depend on  $N$  as well as  $R_g$ . Therefore, the corresponding RPA structure factor for DGCs can be written as

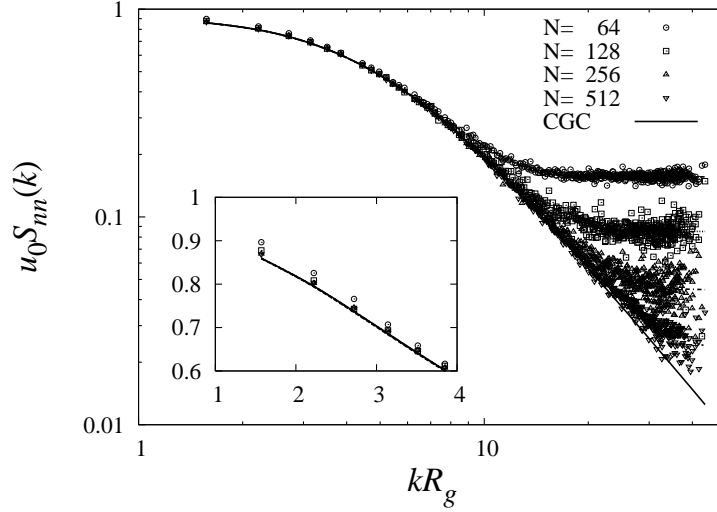
$$u_0 S_{nn}(k, N) \approx \frac{BC \hat{g}_D(k^2 R_g^2, N)}{1 + BC \hat{g}_D(k^2 R_g^2, N)}, \quad (58)$$

where [38]

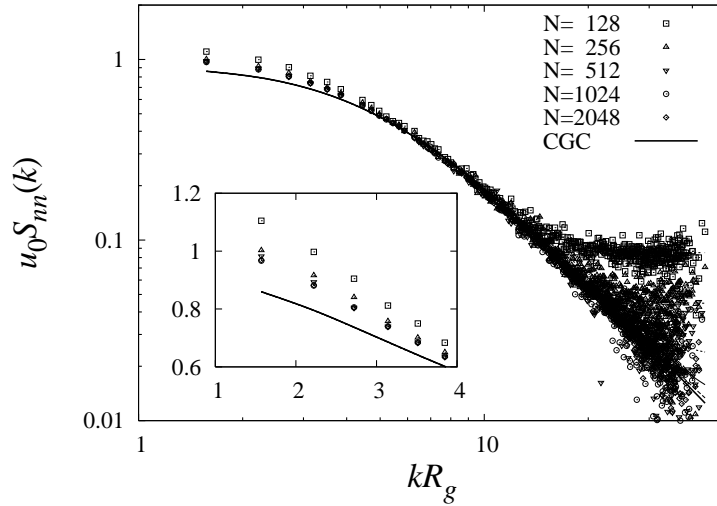
$$\hat{g}_D(k^2 R_g^2, N) = \frac{1}{(N+1)^2} \sum_{i,j=0}^N \exp \left[ -(k R_g)^2 \frac{|i-j|}{N} \right]. \quad (59)$$

RPA segment structure factors for DGCs of various  $N$  are compared with that of the CGC in FIG. 1. At fixed  $BC$ , the low  $k$  behavior of the structure factor, related to the isothermal osmotic compressibility, is independent of the level of discretization of the constituent chain molecules. It is only in the high  $k$  regime (compared with  $2\pi/R_g$ ) where the discrete nature of the DGC model manifests itself by saturating the  $1/k^2$  decay of the structure factor.

As expected, the RPA structure factor proves to be a valid approximation to  $S_{nn}(k)$  as long as the  $w$  field fluctuations are weak and approximately Gaussian. This has been verified by comparing the RPA structure factor to results obtained from FTS, which incorporates the



(a) Dense solution:  $B = 1$  and  $C = 12$



(b) Moderately-dense solution:  $B = 12$  and  $C = 1$

FIG. 2: The segment structure factor in solutions of neutral discrete Gaussian chains: Symbols are FTS results calculated from Eq. (23). Lines are RPA structure factors from FIG. 1. A three dimensional lattice of  $M = 32^3$  sites was employed with periodic boundary conditions. The cell volume was  $V = (4R_g)^3$ .  $u_0$  was varied as  $N$  was changed to keep  $B$  fixed at either 1 or 12.

full field fluctuation spectrum. In FIG. 2, structure factors derived from FTS for two different solution conditions are compared with the RPA structure factor. FIG. 2(a) corresponds to the case of a dense solution ( $C > B$ ) with  $B = 1$  and  $C = 12$ , while FIG. 2(b) describes a moderately-dense solution with  $B = 12$  and  $C = 1$ . However, both share the same RPA

predictions of FIG. 1, because the RPA segment structure factor only depends on the product  $BC$  which is fixed at 12. As FIG. 2(a) shows, there is very good quantitative agreement between RPA structure factors and FTS-derived structure factors when the solution is dense ( $C/B = 12$ ). However, in the moderately-dense regime, as exemplified by FIG. 2(b), the RPA breaks down, especially at low  $k$ . Due to strong excluded volume correlations in this regime, the system evidently has a larger osmotic compressibility than is predicted by the RPA.

Additionally, the FTS results at low  $k$  show that the strength of the  $w$  field fluctuations actually depends on  $N$ . As implied in Eq. (35), the  $w$  field fluctuations tend to increase the osmotic compressibility of the system, and the FTS results indicate that this tendency gets stronger for smaller  $N$  (see insets of low  $k$  regime in FIG. 2). While a discrete chain with  $N \gtrsim 256$  is sufficient to model  $N$ -independent thermodynamic properties in a dense solution with  $C/B = 12$ , a substantially larger  $N$  ( $\gtrsim 1024$ ) is required for  $N$ -independent thermodynamics in a moderately-dense solution of  $B/C = 12$ .

At larger  $k$  and for large  $N$ , we can apply an asymptotic expression for the Debye function,  $\hat{g}_D(k^2 R_g^2) \approx 2/k^2 R_g^2$ , which is highly accurate for  $k R_g > 2\pi$ . Using this approximation, the RPA structure factor for the segment density (Eq. (57)) can be rearranged as

$$\frac{1}{u_0 S_{nn}(k)} \approx 1 + \xi_u^2 k^2, \quad (60)$$

where  $\xi_u$  is the correlation length for segment density. We use Eq. (60) to define  $\xi_u$  even outside of the RPA, but note that the RPA predicts that  $\xi_u = \xi_E$ , where  $\xi_E = R_g/(2BC)^{1/2}$  is the Edwards correlation length. In FIG. 3, segment correlation lengths are estimated from FTS structure factors, which quantitatively agree with a prior FTS study that used an independent method of estimating  $\xi_u$  [34]. Not surprisingly, the Edwards correlation length is a good approximation to the segment correlation length extracted from FTS when the solution is dense. The segment correlation length in a moderately-dense solution, however, is underestimated by the Edwards correlation length.

## B. Correlations in symmetric polycation-polyanion mixtures

In this subsection, density correlations in homogeneous polyelectrolyte solutions are studied with FTS. Unlike the results presented so far for uncharged polymer solutions, charge

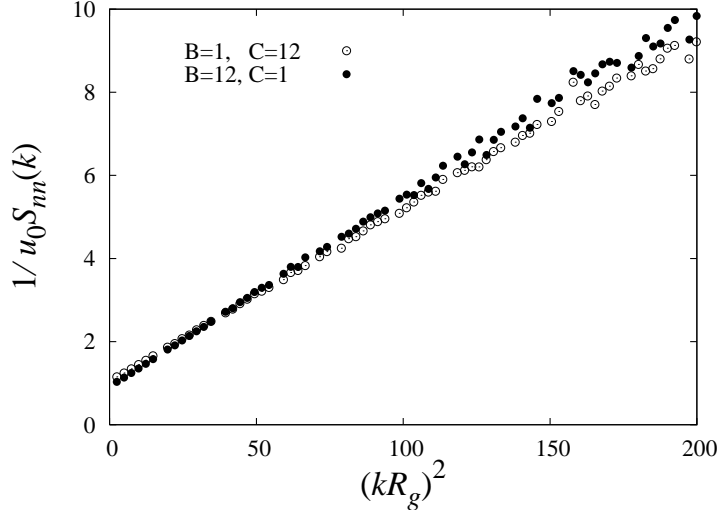


FIG. 3: Inverse structure factor plot used to extract the correlation length for segment density,  $\xi_u$ . According to Eq. (60),  $\xi_u$  can be estimated from the ratio of the slope to intercept in the intermediate  $k$  region of this plot,  $1/R_g < k/2\pi < 1/\xi_u$ . We find that  $\xi_u/R_g = 0.201 \pm 0.0014$  in the case of  $B = 1$  and  $C = 12$ , and  $\xi_u/R_g = 0.225 \pm 0.0016$  for  $B = 12$  and  $C = 1$ . The Edwards correlation length is  $\xi_E/R_g \simeq 0.204$  for  $BC = 12$ . The simulations were conducted on a  $M = 32^3$  lattice with periodic boundary conditions, a system volume of  $V = (4R_g)^3$ , and a chain length of  $N = 1024$ . The linear fit was applied in the regime of  $(kR_g)^2 \in [30, 200]$ .

correlations, as well as segment correlations, are of interest in polyelectrolytes. Specifically, we are interested in the interplay between charge correlations and segment correlations and how they relate to the phenomenon of complex coacervation. In all the FTS results reported in this subsection, the solution was dense ( $C = 12$ ,  $B = 1$ ) and discrete Gaussian chains of  $N = 1024$  were used.

The RPA structure factor of Eq. (57) for the segment density is evidently independent of the charge content in the system; this is a result of decoupling of  $w$  and  $\phi$  fluctuations at the RPA level. It would seem that without a higher-order analysis of fluctuations, it is impossible to guess even the qualitative effect of charge correlations on segment correlations. However, the one loop result for the osmotic pressure does provide some insight. From Eq. (35), the charge correlations are seen to reduce the osmotic pressure of a homogeneous solution, the same effect caused by the segment correlations. Thus, by adding equal and opposite charges to the chains of a neutral polymer solution, we can expect to obtain a solution with increased

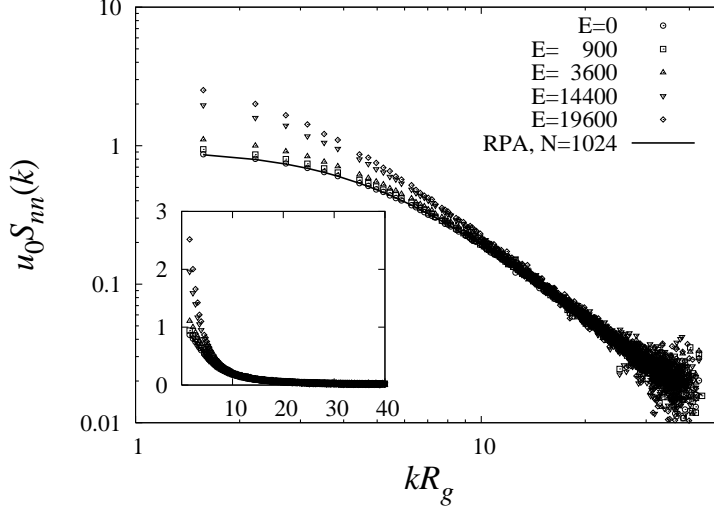


FIG. 4: The segment structure factor in solutions of symmetric polyelectrolytes. The symbols are FTS results and the line is calculated from the RPA result, Eq. (58). The following parameters were used:  $B = 1$ ,  $C = 12$ ,  $N = 1024$ ,  $V = 4 \times 4 \times 4R_g^3$ , and  $M = 32 \times 32 \times 32$ .

osmotic compressibility. This increase in compressibility will in turn be manifest in the low  $k$  behavior of  $S_{nn}(k)$ .

In FIG. 4, segment structure factors for symmetric polyelectrolyte solutions were obtained from FTS. Because the solution is dense, the RPA structure factor is observed to be a good approximation when the polymers are neutral ( $E = 0$ ). However, as the charge density is increased from zero, the FTS results show strong deviations from the RPA structure factor which is independent of  $E$ . The osmotic compressibility increases monotonically with  $E$  and eventually diverges at even higher  $E$ , indicative of a macrophase separation (in this case “complex coacervation”).

Another structure factor of interest in the charged system relates to the charge density correlation. When the  $\phi$  field fluctuations are weak, the RPA formula for the charge density structure factor, Eq. (39), can be combined with Eqs. (33) and (36) to obtain the following approximation:

$$\frac{4\pi l_B}{k^2} S_{cc}(k) \approx \frac{CE\hat{g}_D(k^2 R_g^2)}{k^2 R_g^2 + CE\hat{g}_D(k^2 R_g^2)}. \quad (61)$$

This RPA formula also applies to solutions of discrete Gaussian chains when the modified Debye function of Eq. (59) is substituted for Eq. (30). We see from Eq. (61) that the RPA structure factor for the charge density is completely dictated by the combination parameter



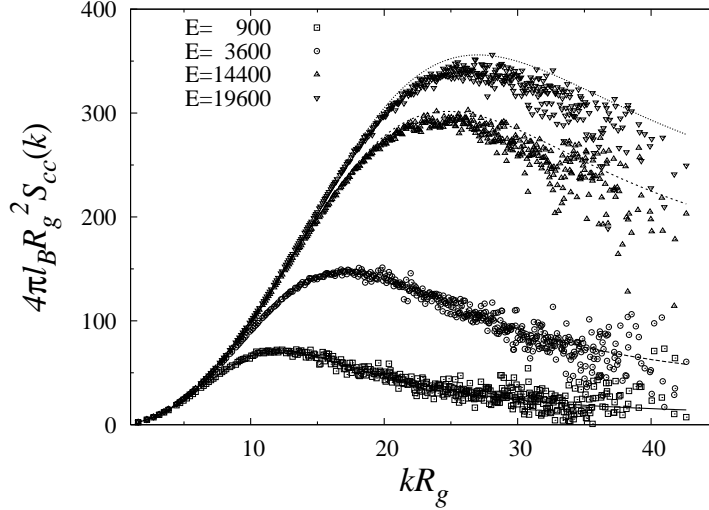


FIG. 5: The charge structure factor in solutions of oppositely charged polyelectrolytes. Symbols are FTS results, while the lines are RPA structure factors calculated from Eq. (61). In the simulations, we vary the parameter  $E$  by changing  $z$  while keeping  $l_B$  constant. The parameters correspond to:  $l_B = R_g/8$ ,  $B = 1$ ,  $C = 12$ ,  $N = 1024$ ,  $V = (4R_g)^3$ , and  $M = 32^3$ .

$CE$ , and is independent of  $B$ .

By again utilizing the asymptotic expression for the Debye function,  $\hat{g}_D(k^2 R_g^2) \approx 2/k^2 R_g^2$ , valid for  $N \gg 1$  and  $kR_g > 2\pi$ , the inversion of Eq. (61) provides

$$\frac{k^2}{4\pi l_B S_{cc}(k)} \approx 1 + \xi_c^4 k^4, \quad (62)$$

which defines a new charge correlation (or screening) length  $\xi_c$ . Explicit use of the RPA formula leads to the result  $\xi_c = \xi_{PE}$ , where  $\xi_{PE} = R_g/(2EC)^{1/4}$ .

Eqn (62) also predicts that  $S_{cc}(k)$  is *maximal* at  $k = 1/\xi_c$ . Note that the correlation length  $\xi_{PE}$  is proportional to the  $-1/4$  power of the segment density, and hence is qualitatively different from the Debye-Hückel length for small ions, which is proportional to the  $-1/2$  power of the ion density. Thus, the attachment of charges to polymer chains creates a coupling between chain conformational statistics and charge density that drastically changes the electrostatic correlation properties of polyelectrolyte solutions compared with a conventional small-ion electrolyte.

In FIG. 5, FTS results for the charge density structure factor are compared with RPA predictions based on Eq. (61). The dimensionless object  $4\pi l_B R_g^2 S_{cc}$ , instead of  $4\pi l_B S_{cc}/k^2$ , is plotted to clearly show the location of the maximum ( $\sim 1/\xi_c$ ) and the screening of charge

density at low  $k$ :  $S_{cc}(k) \sim k^2$ . Although the RPA remains a good approximation at low charge content ( $E = 900, 3600$ ), the deviation between the RPA and FTS becomes noticeable at larger  $E$  and larger  $k$ . As  $E$  increases, the maxima of both the RPA and FTS results shift to higher  $k$ , indicating a shorter screening length consistent with the RPA scaling  $\xi_c \sim (EC)^{-1/4}$ . At  $E = 19600$ , however, the RPA structure factor places the maximum at a somewhat higher value of  $k$  than FTS. In other words, the RPA underestimates the charge correlation length for strongly charged chains. It is also evident that the RPA slightly overestimates the amplitude of charge correlations at large  $E$ . Later, it will be shown that this qualitative observation is consistent with differences observed between phase boundaries deduced from FTS studies and the one-loop analysis.

### C. Complex coacervation: phase diagram

As implied by the diverging osmotic compressibility in FIG. 4, a macrophase separation (complex coacervation) is possible in our field theory model. It was already anticipated in the analytic one-loop correction to the osmotic pressure, Eq. (35), that a phase separation may result from the competition between the positive second virial term from the excluded volume interaction and the negative contribution from charge correlations. The spinodal (single-phase stability limit) is determined by the condition  $\partial\beta p/\partial C = 0$  from the one loop osmotic pressure expression of Eq. (35). With an additional approximation regarding the dilute phase, the one-loop theory can also predict the binodal (the coexistence curve of dilute and coacervate phases). Assuming a supernatant dilute phase free of polyelectrolyte, we can write the binodal equation in the form of  $\beta p = 0$ .

In the context of computer simulations, a rigorous construction of a phase diagram requires a computational technique for accessing the free energy of the system. In the case of particle-based simulations, a variety of free energy estimation methods are available, including thermodynamic integration techniques, Gibbs ensemble and particle insertion methods, and histogram techniques [47, 48]. Such methods, however, are only now emerging for field-based simulations, so here we make a crude estimate of the boundary of the two-phase region in our polyelectrolyte model by monitoring the hysteresis of an order parameter while varying an intensive parameter of the system. The order parameter chosen to characterize complex coacervation is the density difference  $\Delta\rho$  between the dense coacervate phase and

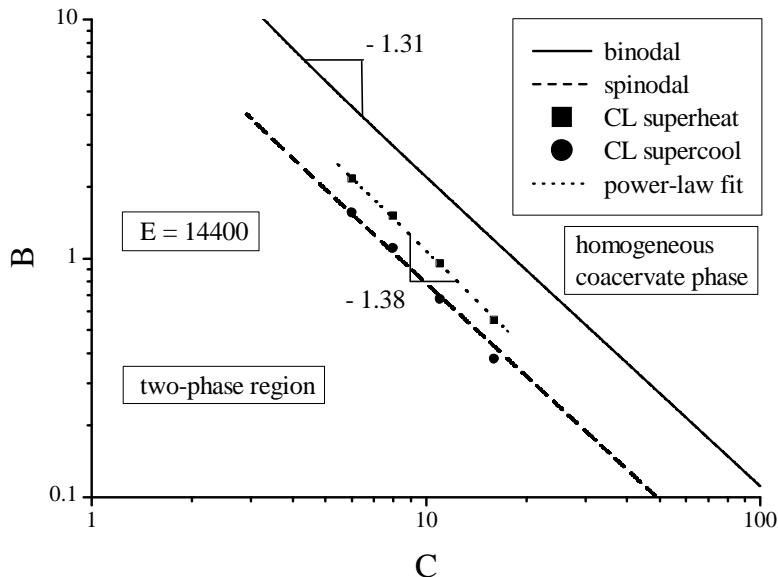


FIG. 6: Phase diagram for the three-dimensional symmetric polyelectrolyte mixture expressed in the coordinates of reduced polymer concentration  $C$  and reduced excluded volume  $B$  at fixed reduced Bjerrum length  $E = 14400$ . Solid and dashed lines are the analytical one-loop binodal and spinodal, respectively. The one-phase region is above and to the right of the lines, and the two-phase region is below and to the left. Symbols are from the examination of the hysteresis in  $\Delta\rho$  using FTS; details of the procedure are explained in the text. FTS data obtained from supercooling simulations (lowering  $B$ ) are denoted by  $\bullet$ , while superheating data are denoted by  $\blacksquare$ . The dotted line is a power-law fit. The error in the numerical data is comparable to the size of the symbols. Numerical simulations were conducted in a cubic cell of size  $(4R_g)^3$  with periodic boundary conditions and with  $N = 384$ .

the dilute phase. Hysteresis is examined while varying the solvent quality  $B$ . For example, consider a homogeneous single phase solution ( $\Delta\rho = 0$ ) at certain values of  $B$ ,  $C$ , and  $E$ . While slowly “cooling” that system by gradually decreasing  $B$  at fixed  $C$  and  $E$ , a sudden jump in  $\Delta\rho$  from zero to a finite value occurs as the system separates into two phases of different densities. The high density phase can be identified as the complex coacervate. On the other hand, upon “heating” the system from the two-phase region by gradually increasing  $B$  at fixed  $C$  and  $E$ , a sudden drop of  $\Delta\rho$  from a finite value to zero is observed as the system exceeds the limit of superheating and remixes into one homogeneous phase. For most phase transitions, the phase coexistence curve is closer to the superheating curve than

to the supercooling curve. Thus, while the superheating and supercooling curves should bracket the transition, we expect that the superheating curve will lie closer to the binodal boundary.

An example of a phase diagram (in 3D) constructed in such a way is provided in Fig. 6. Spinodals and binodals are surfaces in the three-parameter space of the reduced variables  $C$ ,  $B$ , and  $E$ . The figure represents a cross-section of this three-dimensional space by a plane  $E = 14400$ ; hence, the diagram involves only the  $C$  and  $B$  variables. The one-phase region (disordered homogeneous phase) is above and to the right of the lines, and the two-phase region is below and to the left. The tie lines in the two-phase region are horizontal (constant  $B$ ) and connect nearly pure solvent ( $C \approx 0$ ) with a coacervate phase at the binodal concentration. Remarkably, the analytical and numerical results nearly coincide in the high concentration region of the figure, despite the limitations of each method. The numerical results are subject to finite cell size and chain discretization limitations ( $N = 384$ ), while the analytical predictions neglect two-loop and higher order terms in the fluctuation analysis. Nonetheless, our numerical supercooling result practically follows the analytical spinodal, and the analytical binodal yields similar exponent ( $-1.31$ ) as is obtained from a power-law fit to the numerical superheating points ( $-1.38$ ). The over-estimate of the size of the two phase region by the one-loop theory is consistent with the observation in FIG. 5 that the RPA structure factor over-estimates the strength of charge correlations at large  $E$  and hence expands the two-phase region. The overall semi-quantitative agreement between theory and FTS, however, indicates that both approaches have utility for this class of problems.

#### IV. CONCLUSIONS AND PERSPECTIVE

In this paper, we reported on the application of the emerging field-theoretic computer simulation (FTS) technique to a simple model of polyelectrolyte complexation. Specifically, we built and numerically simulated a field theory model of a salt-free solution containing a symmetric mixture of flexible polyanions and polycations in a good solvent. This particular system constitutes a minimal model for the phenomenon of complex coacervation, a type of liquid-liquid phase separation in which a nearly pure solvent phase coexists with second fluid phase (the “coacervate”) that contains the majority of the polyelectrolytes. Theoretically, the symmetric coacervate model is interesting because the workhorse tool of polymer physics,

self-consistent field theory (SCFT), fails to describe the electrostatic effects responsible for coacervation.

Previous analytical work on closely related models of polyelectrolyte mixtures has shown that complex coacervation can be predicted based on calculations that assume weak, Gaussian field fluctuations, i.e. calculations at the one-loop level of fluctuation expansion [21, 22, 23, 24, 25, 26]. However, the reliability of these predictions have remained unclear because analytical techniques for treating more realistic situations of strong charge and excluded volume correlations are lacking. The FTS results of our paper are significant because they can provide numerical data to assess the validity of the RPA, both in terms of its predictions for charge and segment density correlations and for the location of the two-phase envelope. Overall, we have found that the RPA is remarkably robust in its predictions, except at very high charge densities (large values of the parameter  $E$ ) where it overestimates the strength of charge correlations and the size of the two-phase region.

Perhaps more significantly, our results have validated the emerging field theoretic polymer simulation technique as a powerful new tool for examining the structure and thermodynamics of polyelectrolyte systems. FTS can be applied even in situations where the RPA is inapplicable or technically very difficult, such as cases of mesophases formed by weakly charged polymers with hydrophobic backbones or block co-polyelectrolytes [37]. Complexation of charged polymers that also contain neutral blocks or grafts (which can be either hydrophobic or hydrophilic) can also produce inhomogeneous “structured coacervate” phases that are not amenable to study by current theoretical methods [15, 16, 17, 18]. We expect that FTS will prove to be a valuable tool for exploring these and related types of polyelectrolyte systems.

### **Acknowledgments**

The authors are grateful to Fyl Pincus and Kirill Katsov for many valuable discussions and advice. Acknowledgement is made to the Donors of the American Chemical Society Petroleum Research Fund, the Institute for Collaborative Biotechnology, Rhodia Corporation, and the Mitsubishi Chemical Corporation for the support of this research. This work made use of the MRL Computing Facilities supported by the MRSEC Program of the National Science Foundation under award No. DMR05-20415.

- 
- [1] S. F. Edwards, Proc. Phys. Soc. (London) **85**, 613 (1965).
- [2] P. G. de Gennes, Rep. Prog. Phys. **32**, 187 (1969).
- [3] K. F. Freed, Adv. Chem. Phys. **22**, 1 (1972).
- [4] E. Helfand, J. Chem. Phys. **62**, 999 (1975).
- [5] J. L. Barrat and J. Joanny, Adv. Chem. Phys. **94**, 1 (1996).
- [6] J. Borukhov, D. Andelman, and H. Orland, Eur. Phys. J. B **5**, 869 (1998).
- [7] R. R. Netz and D. Andelman, Phys. Rep. **380**, 1 (2003).
- [8] P. G. de Gennes, *Scaling Concepts in Polymer Physics* (Cornell University Press, Ithaca, NY, 1979).
- [9] M. W. Matsen and F. S. Bates, Macromolecules **29**, 1091 (1996).
- [10] F. Schmid, J. Phys.: Cond. Matt. **10**, 8105 (1998).
- [11] E. W. Cochran, C. J. Garcia-Cervera, and G. H. Fredrickson, Macromolecules **39**, 2449 (2006).
- [12] H. G. Bungenberg de Jong and H. R. Kruyt, Proc. Acad. Sci. (Amsterdam) **32**, 849 (1929).
- [13] H. Zhao, C. Sun, R. J. Stewart, and J. H. Waite, J. Bio. Chem. **280**, 42938 (2005).
- [14] J. W. Hong, W. L. Henme, G. E. Keller, M. T. Rinke, and G. C. Bazan, Adv. Mater. **18**, 878 (2006).
- [15] A. Harada and K. Kataoka, Science **283**, 65 (1999).
- [16] S. van der Burgh, A. de Keizer, and M. A. C. Stuart, Langmuir **20**, 1073 (2004).
- [17] E. Y. Kramarenko, A. R. Khokhlov, and P. Reineker, J. Chem. Phys. **119**, 4945 (2003).
- [18] E. Y. Kramarenko, A. R. Khokhlov, and P. Reineker, J. Chem. Phys. **125**, 194902 (2006).
- [19] I. Michaelis, J. T. G. Overbeek, and M. J. Voorn, J. Polym. Sci. **23**, 443 (1957).
- [20] J. T. G. Overbeek and M. J. Voorn, J. Cell. Comp. Physiol. **49S1**, 7 (1957).
- [21] V. Y. Borue and I. Y. Erukhimovich, Macromolecules **21**, 3240 (1988).
- [22] V. Y. Borue and I. Y. Erukhimovich, Macromolecules **23**, 3625 (1990).
- [23] A. Kudlay and M. Olvera de la Cruz, J. Chem. Phys. **120**, 404 (2004).
- [24] A. Kudlay, A. V. Ermoshkin, and M. Olvera de la Cruz, Macromolecules **37**, 9231 (2004).
- [25] M. Castelnovo and J.-F. Joanny, Eur. Phys. J. E **6**, 377 (2001).
- [26] M. Castelnovo and J.-F. Joanny, Macromolecules **35**, 4531 (2002).
- [27] N. N. Oskolkov and I. I. Potemkin, Macromolecules **40**, 8423 (2007).

- [28] G. H. Fredrickson, *The Equilibrium Theory of Inhomogeneous Polymers* (Oxford University Press, Oxford, 2006).
- [29] G. Parisi, Phys. Lett. B **131**, 393 (1983).
- [30] J. R. Klauder, J. Phys. A **16**, L317 (1983).
- [31] V. Ganesan and G. H. Fredrickson, Europhys. Lett. **55(6)**, 814 (2001).
- [32] G. H. Fredrickson, V. Ganesan, and F. Drolet, Macromolecules **35**, 16 (2002).
- [33] D. Duechs, V. Ganesan, G. H. Fredrickson, and F. Schmid, Macromolecules **36**, 9237 (2003).
- [34] A. Alexander-Katz, A. G. Moreira, and G. H. Fredrickson, J. Chem. Phys. **118**, 9030 (2003).
- [35] A. Alexander-Katz, A. G. Moreira, S. W. Sides, and G. H. Fredrickson, J. Chem. Phys. **122**, 014094 (2005).
- [36] G. H. Fredrickson, J. Chem. Phys. **117**, 6810 (2002).
- [37] Y. O. Popov, J. Lee, and G. H. Fredrickson, J. Polym. Sci.: Part B.: Polym. Phys. **45**, 3223 (2007).
- [38] M. Doi and S. F. Edwards, *The Theory of Polymer Dynamics* (Oxford University Press, New York, 1986).
- [39] L. L. Salcedo, J. Math. Phys. **38**, 1710 (1997).
- [40] D. Weingarten, Phys. Rev. Lett. **89**, 240201 (2002).
- [41] H. Gausterer and S. Lee, J. Stat. Phys. **73**, 147 (1993).
- [42] D. Gottlieb and S. A. Orszag, *Numerical Analysis of Spectral Methods: Theory and Applications* (SIAM, Philadelphia, 1977).
- [43] P. E. Kloeden and E. Platen, *Numerical Solution of Stochastic Differential Equations* (Springer-Verlag, Berlin, 1992).
- [44] H. C. Ottinger, *Stochastic Processes in Polymeric Fluids* (Springer-Verlag, Berlin, 1996).
- [45] E. Lennon, G. O. Mohler, M. H. Ceniceros, C. J. García-cervera, and G. H. Fredrickson, SIAM Multiscale Model. Simul. (2008), accepted.
- [46] W. P. Petersen, SIAM J. Numer. Anal. **35**, 1439 (1998).
- [47] M. P. Allen and D. J. Tildesley, *Computer simulation of liquids* (Oxford University Press, 1989).
- [48] D. Frenkel and B. Smit, *Understanding molecular simulation* (Academic Press, 2001).

FIG. 1: RPA structure factor for the segment density when  $BC = 12$ . Segment structure factors for several values of  $N$ , calculated from Eq. (58), are compared with the result based on the continuous Gaussian chain (CGC), cf. Eq. (57).

FIG. 2: The segment structure factor in solutions of neutral discrete Gaussian chains: Symbols are FTS results calculated from Eq. (23). Lines are RPA structure factors from FIG. 1. A three dimensional lattice of  $M = 32^3$  sites was employed with periodic boundary conditions. The cell volume was  $V = (4R_g)^3$ .  $u_0$  was varied as  $N$  was changed to keep  $B$  fixed at either 1 or 12.

FIG. 3: Inverse structure factor plot used to extract the correlation length for segment density,  $\xi_u$ . According to Eq. (60),  $\xi_u$  can be estimated from the ratio of the slope to intercept in the intermediate  $k$  region of this plot,  $1/R_g < k/2\pi < 1/\xi_u$ . We find that  $\xi_u/R_g = 0.201 \pm 0.0014$  in the case of  $B = 1$  and  $C = 12$ , and  $\xi_u/R_g = 0.225 \pm 0.0016$  for  $B = 12$  and  $C = 1$ . The Edwards correlation length is  $\xi_E/R_g \simeq 0.204$  for  $BC = 12$ . The simulations were conducted on a  $M = 32^3$  lattice with periodic boundary conditions, a system volume of  $V = (4R_g)^3$ , and a chain length of  $N = 1024$ . The linear fit was applied in the regime of  $(kR_g)^2 \in [30, 200]$ .

FIG. 4: The segment structure factor in solutions of symmetric polyelectrolytes. The symbols are FTS results and the line is calculated from the RPA result, Eq. (58). The following parameters were used:  $B = 1$ ,  $C = 12$ ,  $N = 1024$ ,  $V = 4 \times 4 \times 4R_g^3$ , and  $M = 32 \times 32 \times 32$ .

FIG. 5: The charge structure factor in solutions of oppositely charged polyelectrolytes. Symbols are FTS results, while the lines are RPA structure factors calculated from Eq. (61). In the simulations, we vary the parameter  $E$  by changing  $z$  while keeping  $l_B$  constant. The parameters correspond to:  $l_B = R_g/8$ ,  $B = 1$ ,  $C = 12$ ,  $N = 1024$ ,  $V = (4R_g)^3$ , and  $M = 32^3$ .

FIG. 6: Phase diagram for the three-dimensional symmetric polyelectrolyte mixture expressed in the coordinates of reduced polymer concentration  $C$  and reduced excluded volume  $B$  at fixed reduced Bjerrum length  $E = 14400$ . Solid and dashed lines are the analytical one-loop binodal and spinodal, respectively. The one-phase region is above and



to the right of the lines, and the two-phase region is below and to the left. Symbols are from the examination of the hysteresis in  $\Delta\rho$  using FTS; details of the procedure are explained in the text. FTS data obtained from supercooling simulations (lowering  $B$ ) are denoted by  $\bullet$ , while superheating data are denoted by  $\blacksquare$ . The dotted line is a power-law fit. The error in the numerical data is comparable to the size of the symbols. Numerical simulations were conducted in a cubic cell of size  $(4R_g)^3$  with periodic boundary conditions and with  $N = 384$ .